**Citation (APA)**
Kopka, T., Coraddu, A., & Polinder, H. (2026). Modular Energy Management Via Distributed and Predictive Optimization for Fuel Cell-Battery Shipboard Microgrids. *IEEE Open Journal of the Industrial Electronics Society*, *7*, 1155-1171.
https://doi.org/10.1109/OJIES.2026.3710800

Received 6 May 2026; revised 22 June 2026; accepted 3 July 2026. Date of publication 6 July 2026;
date of current version 20 July 2026. The review of this article was arranged by Associate Editor Danilo I. Brandao.

*Digital Object Identifier 10.1109/OJIES.2026.3710800*

# Modular Energy Management via Distributed and Predictive Optimization for Fuel Cell-Battery Shipboard Microgrids

**TIMON KOPKA , ANDREA CORADDU (Senior Member, IEEE), AND HENK POLINDER (Senior Member, IEEE)**

Department of Maritime and Transport Technology, Delft University of Technology, 2628 CD Delft, The Netherlands

CORRESPONDING AUTHOR: TIMON KOPKA (e-mail: t.kopka@tudelft.nl).

This work was supported by the project *Sustainable Hydrogen Integrated Propulsion Drives (SH2IPDRIVE)*, which has received funding from RvO (reference number MOB21013), through the RDM regulation of the Ministry of Economic Affairs and Climate Policy.

**ABSTRACT** Electrification of ship power systems plays a central role in the mobility transition toward sustainable transportation. The integration of a large number of components with distinct characteristics into a shipboard microgrid benefits from a modular design and standardized interfaces. Key challenges lie in the variety of component characteristics, and an evolution of parameters during the power system operation. Further, topology alterations can occur over time, requiring a reformulation of the optimal power dispatch problem. Accordingly, a modular energy management strategy must be adaptive to these changes. This work explores a distributed energy management architecture with a central coordinating agent, realized via Lagrangian dual decomposition and a gradient-based solver. This architecture ensures both local feasibility while reaching global optimality and a power balance through a consensus mechanism. Parameter changes are incorporated in local cost functions, making extensive data exchange with a central unit obsolete. Handling a variable number of power system components, this approach is resilient to component faults, topology redesigns, and component degradation. The method is applied to a fuel-cell battery hybrid harbor tug equipped with multiple parallel modules with unique ratings and state-of-health. The energy management strategy minimizes total operating costs, based on hydrogen fuel consumption and cell degradation. Extensive mission simulations show similar performance for the distributed approach and a centralized equivalent. The predictive strategy is demonstrably superior to instantaneous optimization, yielding a cost reduction of 18.3% with a 15 min prediction horizon. The model predictive control performance increases with the horizon length, reducing operation costs by an additional 6.0% at 60 min. In addition, a local decision-making heuristic shows promising potential for the cell degradation via optimized timing of ON- and OFF switching. At 15 min, this reduces operation costs by 3.0% and at 60 min by 12.7%. Finally, the distributed optimization is deployed on real-time target machines to showcase the applicability of the approach on actual controller and communication hardware.

**INDEX TERMS** Distributed optimization, energy management, fuel cells, predictive control, real-time simulation, shipboard power systems.

## I. INTRODUCTION

The design of marine vessels sees a shift toward the electrification of the shipboard power system (SPS). This facilitates the integration of novel technologies, such as fuel cell (FC) [1], energy storage system (ESS) [2], intermittent power generation, as well as electric propulsion and service equipment [3]. The electric distribution interconnects all system components and increases the operational flexibility, especially regarding the power flows between devices. The increased system complexity makes the coordination of all energy resources a key challenge [4]. Whereas AC distribution is conventionally used in electric ships, DC distribution technology is receiving increasing interest as a solution to tie heterogeneous components together into a shipboard DC microgrid [5]. Interfacing components via power electronics converters increases the controllability of power flows. This further supports the separation of component-level from system-level control, by making synchronization requirements and speed restrictions, as present in AC systems, obsolete [6]. With an increased amount of DC sources (FC, batteries, etc.), the reduction of conversion stages is kept minimal, further increasing system efficiency. The increased flexibility is in line with an observed trend toward modularization and distribution of generation and storage units [7]. Furthermore, increasing importance is attributed to the decarbonization of SPS, for which hydrogen FC offer a feasible solution [1]. The suitability of DC distribution for FC-battery SPS designs is shown in [8]. Given this context, we investigate methods for the minimization of operational costs of hydrogen FC-based SPS. The main drivers are the hydrogen cost and the effects of FC degradation [9], taking into account the unique challenges in maritime environments [10].

Automatic control for the energy management on-board maritime vessels is increasingly adopting optimization-based strategies [11]. The most widespread method for instantaneous optimization with a hybrid energy system (as described in [12]) is equivalent consumption minimization strategy (ECMS) [13]. For a diesel-hybrid tugboat, ECMS has been proposed in several works [14], [15]. In [16], this strategy is adopted for a hydrogen FC-based power system incorporating an additional cost-term for FC degradation. An adaptive ECMS implementation aiming for the modular integration of multiple FC and ESS modules is brought forward in [17].

However, the inherent drawback of this strategy is the neglect of any knowledge on future states and operation modes. An instantaneous optimization fails to properly account for dynamic costs and excludes insights on future disturbances, for which model predictive control (MPC) is a common solution [18]. Corresponding approaches in the literature differ strongly in their scope and time-scale. An ECMS that utilizes information (here: a target state-of-charge (SoC) for the ESS) from a mission-scale optimization, is developed in [19], shaping an example of long-term, static optimization. On the other end of the spectrum, in [20] a predictive power management with short-term predictions for a diesel-hybrid tugboat is implemented, focusing on dynamic objectives. A multilevel MPC for efficient long-term power source dispatch and short-term dynamics is presented in [21], whereas the multilevel control in [22] focuses on generator set operation in DC SPS. Predictive energy management, as opposed to the power management and low-level control loops, is often realized via a static, economic dispatch of power sources. The MPC in [23] features a static optimization for fuel consumption in a diesel-electric ship. For a similar vessel, a two-level MPC in [24] handles slow load fluctuations via a static dispatch of generator sets and battery (dis-)charge. In [25], a centralized, degradation-aware MPC for a hybrid tugboat is implemented, however only considering a single FC and battery, and thus not incorporating different characteristics of parallel components.

One further aspect discussed in the literature is the control architecture employed for the energy management. Generally, the energy management strategy (EMS) can be realized as a centralized optimization, assuming full knowledge of parameters and states of all components [25]. However, such a solution requires careful parameterization, a high computational burden, and lacks scalability [26]. An alternative lies in the shift towards a distributed architecture [27]. Distributed control and multi-agent systems offer increased resilience and survivability [28], and automatic reconfiguration capabilities [29]. In [30], the authors note the plug-and-play characteristic of all-electric ships that facilitates the scalability of the power system. To this end, distributed control offers a suitable framework [31]. Moreover, local control algorithms for each agent may be highly complex and tailored to the source [32], which enables an adaptation to each component's characteristics. Based on these attributes, multiagent systems meet the requirements for a modular control framework that handles a multitude of power system components with individual parameters [33]. Further advantageous features of the distributed architecture are the privacy-preservation [31] and the reduction of computational requirements in a centralized unit [27].

A multiagent distributed control for the fuel consumption minimization with multiple diesel generators is investigated in [34]. Lagrangian multipliers are employed in [35] for the economic dispatch of generator sets and ESS in a naval, all-electric ship. The optimum is achieved when all units have the same marginal cost of power generation. Multiple researchers present lambda iteration, a gradient-based method, to solve the Lagrangian dual decomposition. In [36], this is used in a federated architecture for economic dispatch within a microgrid, while a fully distributed application in [37] manages various power generation and storage units. Lagrangian decomposition is demonstrated as a suitable method for optimization in modular system topologies in [38].

In SPS, distributed and multiagent-based approaches have been applied to increase the resilience of naval ships [28] with a focus on power system reconfiguration [39], load management [40], and reserve power allocation [31]. For long-term objectives in ship energy systems, a Lagrangian approach is utilized in [34] for parallel diesel generators. This approach is expanded to a ship-harbor energy system in [41], leveraging the absence of a central coordinator. In distributed optimization, the alternating direction method of multipliers (ADMM) is often proposed as an alternative to lambda iteration, e.g., for the economic dispatch in microgrids [42]. A common prerequisite for both dual decomposition-based and ADMM-based consensus is the convexity of all local cost functions. As already shown in [25], the costs of FC and battery modules can be represented aptly via convex functions over their output power.

Combining distributed and predictive energy management is receiving increasing interest for the control of SPS. For

**TABLE 1. Literature on Distributed Energy Management in Shipboard Power Systems for Optimal Economic Dispatch of Resources**

| | FC | ESS | Predictive | Degradation | Method |
|---|---|---|---|---|---|
| [34] | | | | | $\lambda$-iteration |
| [35] | | X | | | $\lambda$-iteration |
| [27] | | X | | | ADMM |
| [32] | | X | X | (X) | $\lambda$-iteration |
| [45] | | X | X | | ADMM |
| [31] | | X | X | | ADMM |
| This Work | X | X | X | X | $\lambda$-iteration |

a fast-timescale subproblem, distributed optimization via ADMM ensures power servicing constraints as shown in [43]. ADMM for distributed MPC to manage the SoC of ESS in a zonal SPS is proposed in [44] to minimize the load on generators with pulsed loads. A static distributed optimization for an SPS using ADMM is shown for economic dispatch in [45], leveraging short-term load forecasting. However, this work is not considering dynamic limitations and load fluctuations. An MPC formulation in [32] aims at fuel minimization while additionally including a battery degradation cost term. Coordination is realized via Lagrange multipliers while the authors note that local source-dependent optimization algorithms may be highly complex.

Table 1 summarizes research articles that apply distributed methods optimization-based economic dispatch in SPS. Most contributions focus on hybrid architectures, and several adopt predictive control schemes. However, degradation-awareness is only addressed in [32], where a heuristic metric is introduced to account for battery wear. The existing literature does not yet offer an approach that aligns with the desired plug-and-play capability required for the adaptive integration of multiple FC and ESS units with heterogeneous characteristics. To address this gap, this work proposes a distributed, predictive energy management framework for FC–battery SPS, in which FC degradation is explicitly incorporated into the cost function. To this end, the following contributions are made.

1) Distributed implementation of an optimization-based energy management which allows the integration of heterogeneous power system components and an adaptation to their characteristics via local agents.
2) Leveraging load predictions in a predictive energy management for the anticipation and avoidance of increased operating costs due to dynamic operation, as well as an explicit formulation of operational constraints.
3) Definition of a local decision-making heuristic for the state switching of FC modules, allowing a minimization of operating time and undesirable operating points.

The proposed method is compared to a centralized MPC to evaluate the effect of the altered control architecture on the energy management performance. A demonstration at the example of a FC-battery hybrid tugboat highlights the benefits of a predictive, distributed, and optimization-based energy management. For the use case both long-term simulation studies and control implementation on multiple real-time target machines, are presented.

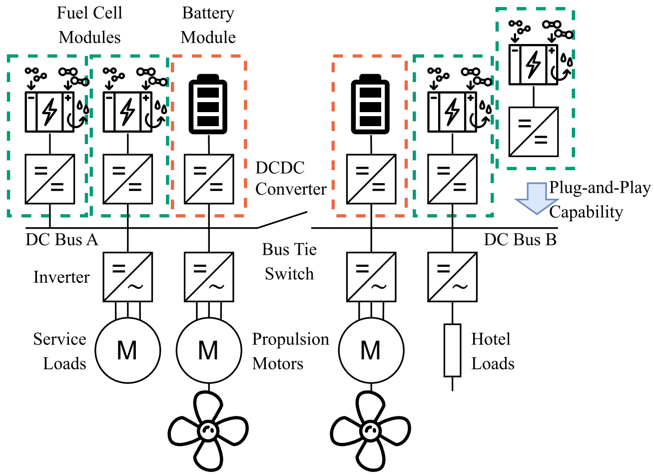


**FIGURE 1. Modular FC-battery shipboard DC microgrid with four FC modules and two battery modules.**

The remainder of this article is organized as follows. Section II briefly describes the power system design and component models. Section III derives the proposed approach for the distributed ECMS and MPC for the control of modular FC-battery SPS and presents algorithms for the implementation in local and centralized controllers. In Section IV, the performance of centralized and distributed energy management strategies as well as the performance of predictive control for different prediction horizons are evaluated numerically. This section further investigates the effect of local FC state decision-making. The deployment of the algorithms on real-time controller hardware and communication network is presented in Section V. Finally, Section VI reviews the contributions made in this work and gives an outlook on future research activities on this topic.

## II. MODULAR POWER SYSTEM

We consider a shipboard DC microgrid whose primary equipment is comprised of FC and battery modules that supply various power-controlled loads. In this work, we study a harbor tug boat with a dual-bus, low-voltage DC distribution system that connects four FC and two ESS modules in total, as shown in Fig. 1. Each of the power generation and energy storage systems is connected to the DC bus via a DC–DC converters, whereas loads are interfaced via inverters, lending full controllability of the power flows in the system. In addition, Fig. 1 highlights the plug-and-play characteristic offered by the DC distribution and power converters, allowing a flexible re-design of the topology by adding or removing modules. The power load is predominantly for propulsion, and in this study follows a fixed trajectory that needs to be met by the cumulative power generation of FC and ESS. A key characteristic of this modular power system is, apart from the flexible number of power system components, the individual characteristics of each module. The power system control is required to accommodate individual component ratings, parameters,

**TABLE 2. FC Degradation Parameters (Per Cell), Adapted from [25]**

| Param. | Description | Value |
|---|---|---|
| $c_{h2}$ | Hydrogen costs | 8 u/kg |
| $c_{fc,capex}$ | System cost | 1500 u/kW |
| $r_{fc,stack}$ | Stack cost ratio | 50 % |
| $r_{eol}$ | Power loss at end-of-life | 10 % |
| $c_{deg}$ | Derived degradation cost | 50.6 u/$\mu$V |
| $p_{lo}$ | Low power threshold | 20 % [1] |
| $p_{hi}$ | High power threshold | 80 % [46] |
| $dv_{hi}$ | High power deg. ($> p_{hi}$) | 10.0 $\mu$V/h [47] |
| $dv_{lo}$ | Low power deg. ($< p_{lo}$) | 8.6 $\mu$V/h [47] |
| $dv_{base}$ | Base degradation | 2.0 $\mu$V/h [48] |
| $dv_{sw}$ | Cyclic degradation | 13.79 $\mu$V [47] |
| $dv_{dyn}$ | Dynamic degradation | 0.5-19 $\mu$V [49] |
| $dt_{dyn}$ | Reference ramp time | 10 s |

and degradation states of all modules while minimizing the total operational cost to service the loads.

### A. FUEL CELLS

Hydrogen proton exchange membrane FC form the main power sources for supplying the SPS. Whereas these FC convert hydrogen efficiently into electric energy, this efficiency drops with an increased power output. Hence, for the energy management it is a key challenge to keep the FC within an efficient operating area. In addition, FC modules are subject to operation-dependent cell degradation, which decreases the performance and eventually requires a replacement of the affected stacks. In this work, we consider the cost of hydrogen, consumed by the FC modules, and the cost of degradation, necessitating a stack replacement, as the main drivers of operational costs for the vessel.

Table 2 lists hydrogen cost and degradation parameters used in this work, with values given in terms of monetary units ([u]). The construction of the FC module degradation function is adapted from [33], and the calculation as well as the quadratic approximation of hydrogen and degradation costs are laid out in [25].

The FC modules are modeled via equivalent circuits, depicted in Fig. 2(a). The FC equivalent circuit consists of a current-dependent voltage source in series with an internal resistance. A degrading FC module is modeled through an increased internal resistance, which leads to an additional voltage drop proportional to the module's output current. This approach is in line with the aging behavior of proton-exchange membrane FC shown in [50]. The state-of-health of a module (given as a relative value) is reflected in the corresponding decrease of the module's output voltage at rated current relative to its value at begin-of-life (BOL). The voltage curve of an exemplary FC module at begin- versus end-of-life, based on manufacturer data from [51], is shown in Fig. 3.

### B. ENERGY STORAGE SYSTEMS

Batteries are used as ESS to complement the specific characteristics of FC, as they are able to alter their power output quickly to match fast load power fluctuations [2]. Furthermore, ESS of sufficient sizing allow for load leveling and strategic charging, supporting the FC modules to operate in more favorable operating points rather than following the load. However, a key challenge for ESS is the management of their SoC, as the amount of stored energy is a limited resource for the energy management. The battery is also modeled using an equivalent circuit, consisting of an SoC-dependent voltage source in series with an internal resistance, and is depicted in Fig. 2(b).

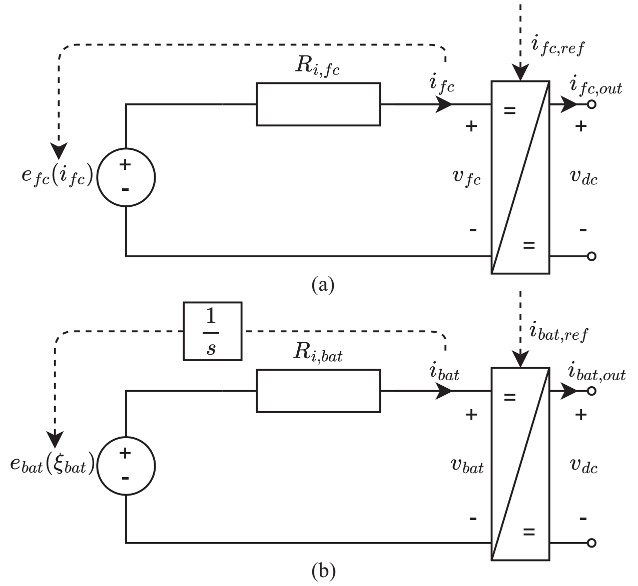


**FIGURE 2.** Equivalent circuit models including power converter for (a) FC module, (b) battery module, adapted from [25].

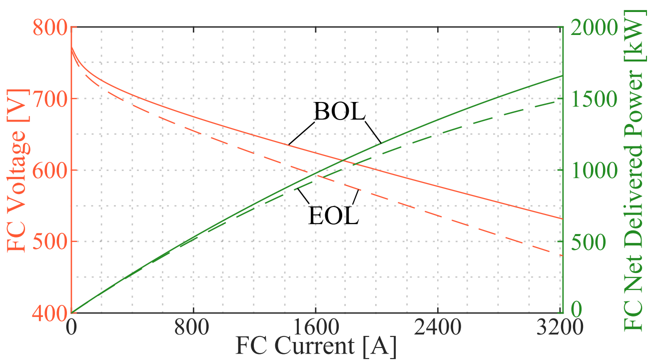


**FIGURE 3.** FC voltage and net output power as functions of output current at begin- and end-of-life, adapted from [25].

### C. DC SYSTEM AND LOADS

The load power $p_{load}$ is modeled as an external disturbance on the system. Its behavior is application-specific and differs in amplitude and volatility, among other factors. The power system components must be selected and sized appropriately for a given ship's load requirements. The main constraint the energy system imposes on the control, is the power balance. This demands that the sum of all components' power outputs must equal $p_{load}$ at all times. As the focus of this article is placed on the energy management, fast transients of the distribution system and power converter controls are neglected.

## III. MODULAR ENERGY MANAGEMENT

This study focuses on the energy management task, responsible for determining the power dispatch for all power system components. This section introduces a generalized approach for the distributed optimization of the energy management in SPS with heterogeneous generation and storage modules with convex cost functions. For this, local optimizers for FC and battery modules, and a system-level coordinator are described. The approach is then extended into a predictive optimization framework. Finally, a nonconvex decision-making heuristic is added to the EMS.

### A. INSTANTANEOUS OPTIMIZATION

We consider a power system equipped with a set of FC $I$ and a set of batteries $J$ that make up all distributed generation modules $M = I \cup J$. Each module's individual cost is a function of the system's parameters, states, and control inputs. In addition, every component is subject to individual constraints, most notably on the power output, power gradient, and battery SoC. Each unit $m \in M$ has an individual cost function $f_m(p_m, x_m)$ that depends on is the unit's power output $p_m$ (decision variable) and a state vector $x_m$. The decision variable is bounded by minimum and maximum power outputs $P_{m,min}$ and $P_{m,max}$. Power loads and intermittent generation pose disturbances on the power system that we aggregate as a scalar $p_{load}$.

#### 1) DUAL DECOMPOSITION

Regarding only one time instant, the energy management's goal is to minimize the total cost of power generation while meeting the power balance constraints:

$$\min_{p_m} \sum_{m \in M} f_m(p_m, x_m) \tag{1}$$

$$s.t. \sum_{m \in M} p_m = p_{load} \tag{2}$$

$$P_{m,min} \leq p_m \leq P_{m,max}, \forall m \in M. \tag{3}$$

This optimization problem is separable via dual decomposition [38], such that each unit solves a local optimization problem given a fixed Lagrange multiplier $\mu$. The multiplier can be interpreted as a price for the output power. Each module maximizes its own utility, while respecting local constraints to maintain local feasibility:

$$\max_{p_m} \mu p_m - f_m(p_m, x_m), \forall m \in M. \tag{4}$$

#### 2) LOCAL OPTIMIZATION PROBLEMS

The operating cost of a FC module $i$ is a function of its power level and power gradient, and incorporates both fuel costs and operation-dependent cell degradation costs. We formulate the costs as a time discrete function with an optimization time period $\Delta t$. Given the power $p_{i,k-1}$ of module $i$ at time $k-1$ as a state, the cost function for transitioning to $p_{i,k}$ at the next time instant is

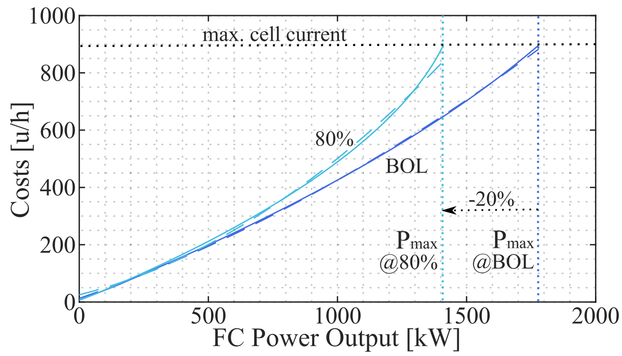


**FIGURE 4.** Cost model (solid) and second-order polynomial approximation (dashed) for PEMFC at BOL (blue) and 80% SoH (turquoise).

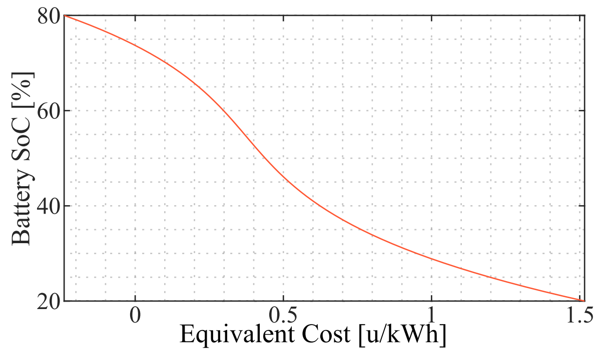


**FIGURE 5.** SoC-dependent equivalent cost of stored energy.

$$f_i(p_{i,k}, p_{i,k-1}) = k_{2,i} p_{i,k}^2 + k_{1,i} p_{i,k} + k_{0,i} + k_{d,i} \frac{(p_{i,k} - p_{i,k-1})^2}{\Delta t} \tag{5}$$

where $k_{x,i}$ are module-specific coefficients that realize a polynomial approximation. It must be noted that the approximation is used only for the system control, whereas its performance is measured against the actual costs. Fig. 4 shows exemplary static cost curves and their second-order polynomial approximations, of a new and an aged FC module. Note that the illustrated decrease to 80% state-of-health is beyond the conventional end-of-life definition of 10% power loss [52].

Similar to a conventional ECMS-approach [13], the stored energy in an ESS is assigned an equivalent cost $\lambda$, which is a function of the module's SoC $\xi_j$. Fig. 5 shows an exemplary case of the value of stored energy. With this, we define the cost function of a battery as

$$f_j(p_{j,k}, \xi_{j,k-1}) = \lambda(\xi_{j,k-1}) \left( p_{j,k} + k_{2,j} p_{j,k}^2 \right) \tag{6}$$

which considers both the cost of discharge or revenue from charging, dependent on the sign of the power output, as well as quadratic power losses. The states denoted with index $k-1$

can be interpreted as the actual value that is currently measured, while values at index $k$ are the decision variables.

Using the local cost functions for FC and battery modules, a distributed ECMS can be derived via dual decomposition. Each FC module has a locally optimal power output $p^*_{i,k}(\mu_k)$ solving its specific optimization problem for the next time step $k$, and based on the current state variable at $k-1$:

$$\max_{p_{i,k}} \mu_k p_{i,k} - f_i(p_{i,k}, p_{i,k-1}). \tag{7}$$

The equivalent problem for a battery module yields $p^*_{j,k}(\mu_k)$:

$$\max_{p_{j,k}} \mu_k p_{j,k} - f_j(p_{j,k}, \xi_{j,k-1}). \tag{8}$$

It must be noted that all modules have additional local constraints on their power output range, power gradient (FC), and SoC range (batteries), that the local optimization steps are subject to.

### 3) GLOBAL FEASIBILITY

For global feasibility, a central coordinator is required to adjust $\mu$, functioning as a system wide price. All modules have convex cost functions, i.e., $p^*_{i,k}$ and $p^*_{j,k}$ that are nondecreasing in $\mu$. More specifically, $p^*_{i,k}$ and $p^*_{j,k}$ are monotonously increasing within their operational limits. In addition, operational requirements demand that the total generation capacity must be larger than the maximum load power, meaning that for any allowable load power there must be at least one module that is not at capacity. In consequence, the total power generation, as the sum of all modules' optimal power outputs, is monotonously increasing for all relevant load power levels and associated values of $\mu$:

$$\sum_{i\in I} \frac{dp^*_{i,k}}{d\mu_k} + \sum_{j\in J} \frac{dp^*_{j,k}}{d\mu_k} > 0. \tag{9}$$

Accordingly, using a gradient-based method, e.g., lambda iteration, lets us find a value $\mu^*$ that satisfies the power balance constraint:

$$\sum_{m\in M} p_m(\mu^*) = p_{load}. \tag{10}$$

## B. PREDICTIVE OPTIMIZATION

Using time-series forecasting to predict the future load [53], a set of predictions $\hat{p}_{load,k} \forall k \in [1, \ldots, N_h]$ with prediction horizon $N_h$ can be obtained. The forecasting method, making use of extreme gradient boosting (XGBoost) combined with a time series foundation model, is described in more detail in [25]. An expansion of the problem formulation for a series of discrete time intervals allows the optimization over the prediction horizon for the distributed system.

### 1) LOCAL OPTIMIZATION PROBLEMS

The instantaneous formulations of the local objective functions are extended to capture the costs of each module over a series of discrete time steps. For the ESS, we introduce the terminal battery energy $E_{j,N_h}$ and terminal SoC $\xi_{j,N_h}$ in the optimization formulation. This allows us to assign a cost to the remaining battery energy at the end of the optimization interval. Accordingly, the predictive objective functions for FC and battery modules are formulated as

$$\max_{p_{i,k}} \sum_{k=1}^{N_h} \mu_k p_{i,k} - f_i(p_{i,k}, p_{i,k-1}) \tag{11}$$

$$\max_{p_{j,k}} \sum_{k=1}^{N_h} \mu_k p_{j,k} - f_j(p_{j,k}, \xi_{j,N_h}) + \lambda(\xi_{j,N_h}) E_{j,N_h} \tag{12}$$

where $p_{i,0}$ denotes the FC power at time of optimization. Note that the battery cost function $f_j$ takes the terminal SoC as an argument rather than the value corresponding to the respective time step. Equations (11) and (12), are subject to power and power gradient or SoC limits, as well as the module's state dynamics, as described in [25].

### 2) PRICE ADJUSTMENT

We can interpret the local decision $p^*_{m,k}(\mu_k)$ as a power bid, responding to the externally set market price $\mu_k$. It is the central coordinators' task to adjust the price such that the power balance constraint is fulfilled at each for each time step $k \in [1, \ldots, N_h]$.. Due to the convexity of local functions, each $\mu_k$ can be adjusted via a dual gradient ascent approach until the power balance constraint is fulfilled. That is, there is an equilibrium for a vector of optimal Lagrange multipliers $\mu^*_k$ where the total distributed power generation $\sum_{m\in M} p^*_m(\mu_k)$ is equal to the load. With an iterative approach, we are looking for a value that is sufficiently close to this equilibrium:

$$\epsilon_k := |\hat{p}_{load,k} - \sum_{m\in M} p^*_m(\mu_k)| \leq \varepsilon \quad \forall k \in N_h \tag{13}$$

where $\varepsilon$ defines a small tolerance around the equilibrium.

The distributed MPC is solved iteratively following Algorithms 1 and 2. A central coordinator adjusts each $\mu_k$ individually for time instant $k$ until each module bids a discrete power trajectory such that the power balance constraint is below the tolerance threshold $\varepsilon$ for each $k$. The tasks are divided such that the central coordinator broadcasts $\mu_k$ to all modules. The modules, in return, run the local optimization in Algorithm 2 to obtain $p^*_m$ and share it with the central coordinator. The central coordinator iteratively updates and shares $\mu_k$ and collects all updated $p^*_m$ according to Algorithm 1 until the distributed optimization is converged. Accordingly, an individual market price is established at each time instant.

A generic FC-battery power system topology and the distribution of local and global optimization tasks is shown in Fig. 6. From the system perspective, the type and state of each unit is irrelevant as this information is included in the bids from each module. For the system level optimization, it is sufficient to iteratively update $\mu_k$ until either a convergence criterion is fulfilled or a maximum number of iterations is reached. The price adjustment algorithm, as shown in Algorithm 1, is embedded in a central coordinator that broadcasts $\mu_k$ and sends a trigger signal to request power bids

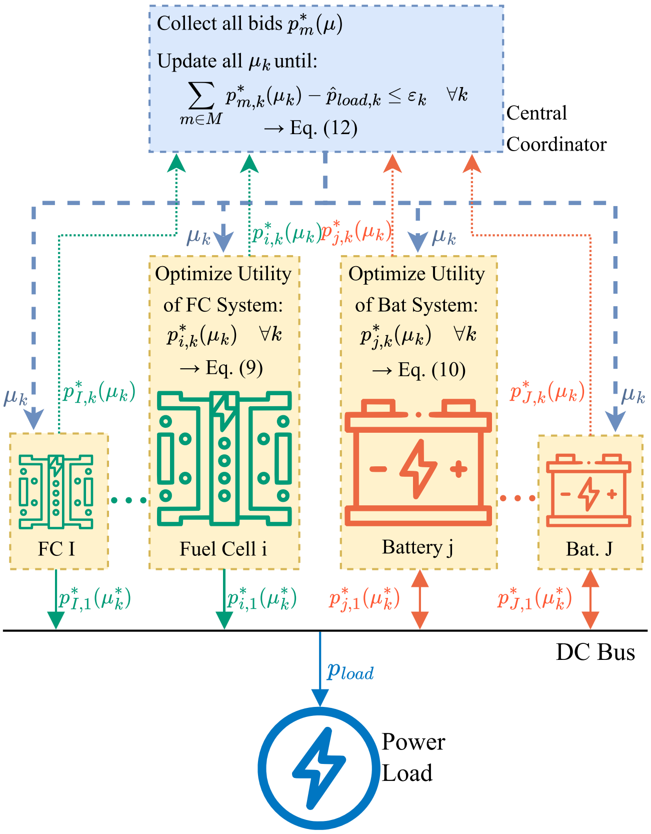


**FIGURE 6.** Control architecture for distributed optimization of modular FC-battery power system via price adjustment.

**Algorithm 1:** Price Adjustment by Central Coordinator.

**Input:** $p^*_{m,k}$, $\hat{p}_{load,k}$
- **if** New Optimization **then**
  - $it \leftarrow 0$
  - $\mu_k \leftarrow \mu^*_{k,prev}$ {Start with Previous Equilibrium Price}
  - Send trigger
  - **return**
- **end if**
- $\epsilon_k \leftarrow \hat{p}_{load,k} - \sum_{m\in M} p^*_{m,k}$
- **if** $\epsilon_k \le \varepsilon$ **or** $it > it_{max}$ **then**
  - Stop trigger {Converged or Max. Iterations Reached}
  - **return**
- **end if**
- $it \leftarrow it + 1$
- $\mu_k \leftarrow \mu_k + \alpha \hat{\nabla}_\mu \epsilon_k$ {Adjust Price}
- Send trigger
- **return**

**Output:** $\mu_k$, trigger

**Algorithm 2:** Local Bidding by Distributed Controllers.

**Input:** $\mu_k$, trigger
- **if** trigger **then**
  - $p^*_{m,k} \leftarrow$ (11) and (12) {Optimal bid by Unit $m$}
- **end if**

**Output:** $p^*_{m,k}$

from all distributed modules. The parameter $\hat{\nabla}_\mu$ is a gradient estimate for the change in price over change in total power bid, $\alpha$ is a factor for the price adjustment step width, $\varepsilon$ is the convergence tolerance, and $it$ and $it_{max}$ are iteration counter and maximum number of iterations, respectively. Upon receiving a trigger signal, each distributed unit updates its power bid according to Algorithm 2. While not satisfying (13), $\mu_k$ is updated according to

$$\mu_{k,it+1} = \mu_{k,it} + \alpha \hat{\nabla}_\mu \left( \hat{p}_{load,k} - \sum_{m\in M} p^*_{m,k} \right) \tag{14}$$

where $it$ is the iteration number of the update step. For gradient-based methods to work effectively, it is ideal to have the gradients at the current operating point available. To avoid a large amount of transmitted data, the distributed modules only share the bid for the currently shared price. It is then up to the central coordinator to update $\mu_k$ according to (13) while balancing convergence speed and stability. For this, it uses the estimate $\hat{\nabla}_\mu$, which approximates the average gradient over all $k$ intervals:

$$E[\hat{\nabla}_\mu] = \frac{1}{N_h} \sum_{k=1}^{N_h} \frac{d\mu_k}{dp_{tot,k}(\mu_k)}. \tag{15}$$

### 3) FUEL CELL STATE LOGIC

In [54], it was generally assumed that all FC are switched ON by default during a mission. To paint a complete picture of the power system operation, the start-up and shutdown of each FC module needs to be included in the energy management strategy. In [33], it has been shown that time-optimized ON–OFFstate switching of individual modules can significantly support in the reduction of operating costs. Each ON-switching action is penalized with a fixed cell voltage deterioration, whereas the reduced running time reduces the cell degradation. To preserve the modularity of the distributed EMS in this work, we propose the implementation of a local state switching logic for each agent. In the distributed predictive EMS, the state command $z_{i,ref}$ is determined based on the bids $p^*_{i,k}$ computed by each FC agent. The state reference must be computed outside of a regular optimization instance lest an integer-valued decision variable is introduced to the problem. Hence, the ON–OFFdecision is made only after an optimization sequence is complete, and is applied starting with the next optimization instance. The decision further needs to be subject to a hysteresis to avoid ON–OFFtoggling at each optimization instance.

The system switches ON if the optimal bid $p^*_{i,k}$ is larger than the threshold $p_{i,on}$ in at least $n_{on}$ prediction intervals. Contrary,

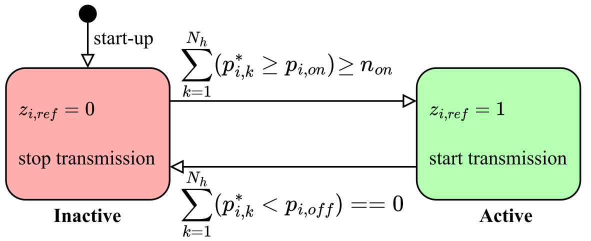


**FIGURE 7.** Local ON–OFF switching logic for FC module.

**TABLE 3.** Default Simulation and Optimization Parameters

| Parameter | Description | Value |
|---|---|---|
| $T_{sim}$ | Simulation step size | 10 ms |
| $T_{com}$ | Communication step size | 100 ms |
| $T_{opt}$ | Optimization step size | 5 s |
| $T_{mpc}$ | MPC optimization interval | 30 s |
| $N_h$ | Optimization horizon | 30 |
| $\varepsilon$ | Constraint tolerance | 10 kW |
| $it_{max}$ | Maximum iterations | 45 |
| $\alpha$ | Descent step size (decreasing) | 0.7-0.07 |
| $\xi_{min}/\xi_{max}$ | Min./Max. battery SoC | 20/80 % |
| $\dot{p}_{fc,max}$ | Max. FC power gradient | $0.05 P_i SoH_i \mathrm{s}^{-1}$ |

the state reference toggles OFF when all $p^*_{i,k}$ are below a minimum value $p_{i,off}$. The state machine for each FC module is visualized in Fig. 7. While a FC module is OFF ($z_{i,ref} = 0$), the agent is not sharing its bids with the central coordinator. Thus, the module is not participating in the power dispatch. When the module switches OFF, it ramps down its power output with a fixed gradient. A disadvantage of increased switching instances lies in increased degradation. Table 2 lists a fixed cell voltage loss $dv_{sw}$ for cyclic degradation, arising from each ON-switching instance.

## IV. NUMERICAL INVESTIGATIONS

We investigate a tugboat whose power system design and operational data are described in [25]. The measurements have been cleaned and parsed into distinct mission profiles. For evaluating the performance of different strategies, we simulate the power system operation for a total of 167 missions recorded over the course of several months. The performance of a specific EMS implementation is evaluated based on the total accumulated cost for hydrogen consumption and degradation, using MATLAB/Simulink simulations. This section features a number of investigations, comparing the performance of centralized and distributed architectures, and investigating the effect of parameterization on the performance of the distributed, predictive energy management.

### A. IMPLEMENTATION

The implementation of the proposed EMS, low-level controllers, and power system simulations requires some considerations. These are described and evaluated in the following.

*Time scales:* The distributed ECMS and MPC algorithms, low-level controllers, and possibly the power system simulation, require digital implementation. The various tasks of the simulation and control algorithms are running at different time steps, as listed in Table 3. The fastest dynamics are present in the simulation of the physical system and the primary control layer, running at $T_{sim}$. Testing on physical hardware presumably requires even faster low-level controllers, depending on switching frequency and current control bandwidths. Each optimization instance is initiated regularly with time interval $T_{opt}$. The MPC optimizes over $N_h$ discrete intervals with an interval length of $T_{mpc}$. Each iteration of the distributed ECMS or MPC is completed at a rate of $T_{com}$, matching the communication bandwidth. The maximum number of iterations $it_{max}$ is set such that an optimization instance is finished before the next optimization is triggered. To reduce the delay caused by a high number of iterations, all modules' power references are updated already during the optimization using the intermediate power bids of the ongoing optimization.

*Initialization:* A suitable initialization of each optimization instance is crucial for the performance of the distributed optimization, considering the number of required iterations. While $T_{opt}$ is significantly smaller than $T_{mpc}$, as realized in this work, initializing a new optimization with the final dual variables of the previous optimization instance is expected to minimize the number of required iterations. If $T_{opt}$ approaches the value of $T_{mpc}$, an index shift or interpolation of values may lead to improved performance. For $T_{opt} = T_{mpc}$, the index shift for a new optimization would assign $\mu_k = \mu_{k+1} \forall k = [1, .., N-1]$.

*Equivalent cost parameterization:* As described in Section III, the stored energy in batteries is assigned an SoC-dependent equivalent cost $\lambda$. In the objective function (12), this term is a function of the SoC at the end of the horizon. Since the terminal SoC depends on the control input of all optimization intervals, the optimization complexity increases significantly. To mitigate this, $\lambda$ is fixed to a constant value within each optimization and is derived from the terminal SoC of the previous optimization instance. This is viable, given that $\mu_k$ is updated in sufficiently small steps. Accordingly, difference of the terminal SoC between subsequent optimization instances, is minor. To further stabilize the behavior of the distributed optimization, $\lambda$ is passed through a low-pass filter with a time constant of several seconds. Doing so avoids unstable bidding behaviors of multiple ESS. The low-pass filter lets all ESS find a consensus on an optimal terminal SoC, and thereby on an optimal equivalent cost of energy for a given optimization horizon.

*Gradient Estimation:* For a proper and stable convergence behavior, the update of the dual variables relies on the estimate of the global power bid gradient. In practice, the real gradient is unknown, unless explicitly shared by the agents, increasing the communication overhead and relaxing privacy conservation. In this work, the gradient is approximated based on the values of the dual variables and total power bids recorded over an optimization instance. Using these data-points, the gradient is approximated using linear regression with a least square

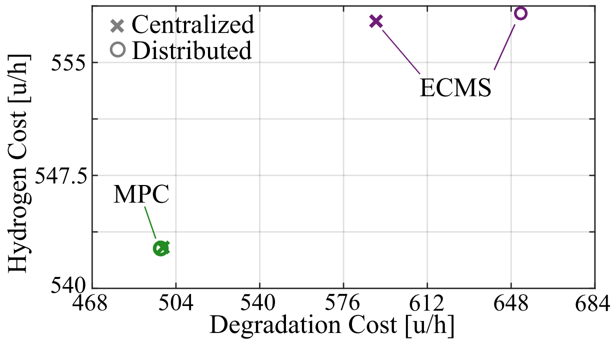


**FIGURE 8.** Hydrogen and degradation costs for all mission profiles with centralized versus distributed implementations of ECMS and MPC.

error approach. To avoid unstable behavior, the gradient estimate is checked for feasibility and diffused with the previous gradient estimate.

The value of $\alpha$ must be strictly smaller than 1.0. Constant values between 0.3–0.7 have shown adequate convergence behavior. To further improve the convergence behavior by enforcing large steps in early iterations and smaller steps close around the solution, the step size is decreased for each iteration, with up to one order of magnitude at the final iteration.

*Real-time power balancing:* The EMS determines optimal power references for each module, averaged over the length of each MPC interval. In fact, the load changes continuous, yielding an imbalance between instantaneous demand and optimized power dispatch. This is compensated by fast-acting voltage controllers deployed in the battery modules, which realize the current sharing according to [55]. The battery modules dynamically adjust their available power based on their maximum rating and their power bid, and accordingly their power sharing gain is adjusted continuously to the operating conditions. It is key to do so for unpredicted load spikes not to lead to an overexertion of a battery system beyond its capacity.

### B. CENTRAL VERSUS DISTRIBUTED

Initially, we consider a power system with only one FC and one battery, allowing the implementation of the centralized approach outlined in [25]. This article describes the power system design and a centralized ECMS and MPC for this case. The aim is to compare the performance of the centralized ECMS and MPC from [25] with the distributed strategy proposed in our study.

Fig. 8 shows the accumulated costs for hydrogen and cell degradation over all 167 simulated mission profiles. Results show nearly identical performance for centralized and distributed implementations of the MPC.

The comparison for ECMS strategies shows close results for the hydrogen costs. Only the degradation is higher with the distributed architecture, which can mainly be attributed to increased dynamic degradation effects. A reason for this lies in small deviations between consecutive optimization instances due to numerical tolerances in the convergence algorithm.

**TABLE 4.** FC and Battery Parameters of Modular Power System

| Parameter | Description | Value |
|---|---|---|
| $P_{fc,A}$ | Max. power FC A at BOL | 1780 kW |
| $SoH_{fc,A}$ | State-of-health of FC A | 100 % |
| $P_{fc,B}$ | Max. power FC B at BOL | 1780 kW |
| $SoH_{fc,B}$ | State-of-health of FC B | 80 % |
| $P_{fc,C}$ | Max. power FC C at BOL | 445 kW |
| $SoH_{fc,C}$ | State-of-health of FC C | 85 % |
| $P_{fc,D}$ | Max. power FC D at BOL | 445 kW |
| $SoH_{fc,D}$ | State-of-health of FC D | 95 % |
| $E_{bat,A}$ | Energy capacity battery A | 1000 kWh |
| $R_{i,A}$ | Inner resistance battery A | 19.2 mΩ |
| $E_{bat,B}$ | Energy capacity battery B | 250 kWh |
| $R_{i,B}$ | Inner resistance battery B | 15.4 mΩ |

This can be alleviated by tightening such tolerances at the expense of convergence behavior. However, results show that this is not present with the predictive strategy, which is the primal subject in this investigation.

This comparison underscores the ability of the distributed architecture to produce the same performance as a centralized implementation, but with the added benefits of the distributed architecture.

### C. MODULAR SYSTEM TOPOLOGY

Next, we consider a system layout that reflects the modular design of modern, zero-emission SPS. The power system is equipped with four FC modules and two battery energy storage systems. Each FC module has an individual power rating and aging state, influencing its polarization curve. Each battery has an individual capacity and differs in cell-specific internal resistance. Accordingly each unit's cost function is unique, which should be reflected in its operation. The parameters of the system components are listed in Table 4. Conventionally, FC systems are considered to reach their end-of-life at 90% state-of-health [52]. However, to explore further operation of modules beyond this point and to highlight discrepancies between local cost functions, we include FC modules who have passed the conventional end-of-life threshold.

### D. PREDICTIVE OPTIMIZATION

The results of one exemplary mission profile using the distributed MPC with a prediction horizon of 15 min are shown in Fig. 9. It can be seen that the FC operate according to their respective marginal cost curves, whereas the power gradients are kept relatively low [Fig. 9(b)]. Among the batteries, the SoC are kept balanced while it is evident that battery B, which has a lower resistance relative to its capacity than battery A, is used more dynamically [Fig. 9(c)]. The evolution of the optimal price in Fig. 9(d) gives an indication of the marginal energy cost at a given point in time. The bids for time instances over the prediction horizon additionally give an indication of the future cost. The latter can potentially serve as an input for the load management. Finally, Fig. 9(e) shows that the number of iterations required for completing each optimization is low, meaning that the needed data traffic

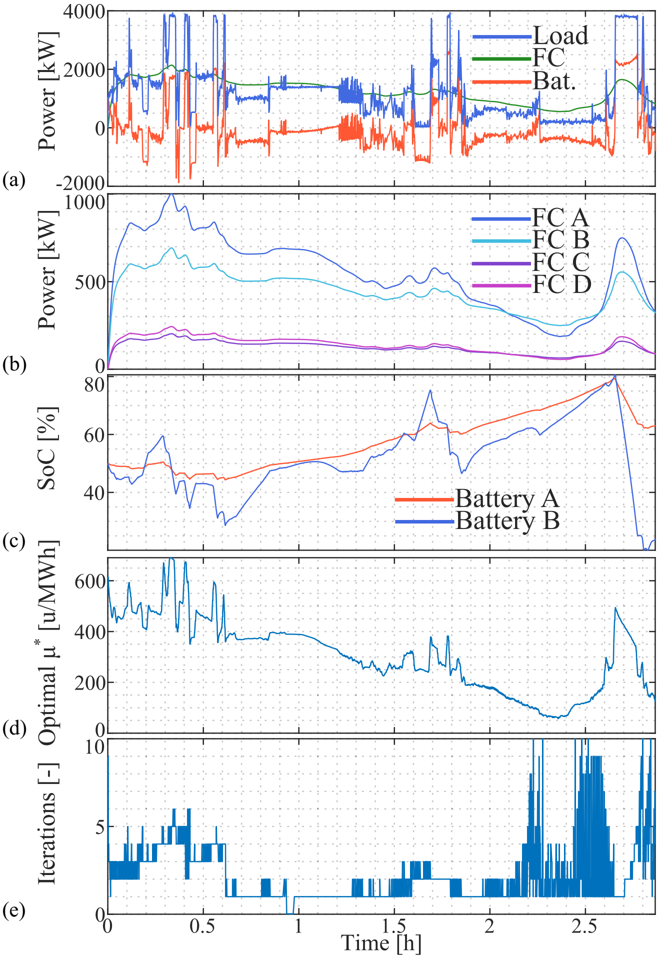


FIGURE 9. Exemplary results for one mission profile with distributed MPC with 15 min load forecasting, showing (a) the total power split, (b) FC power per module, (c) battery SoC per module, (d) the optimal price, (e) iterations required for solving the optimization.

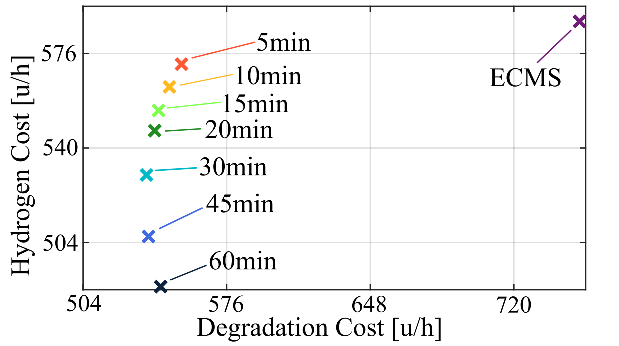


FIGURE 10. Accumulated hydrogen and degradation costs with distributed ECMS, and distributed MPC with different prediction horizons.

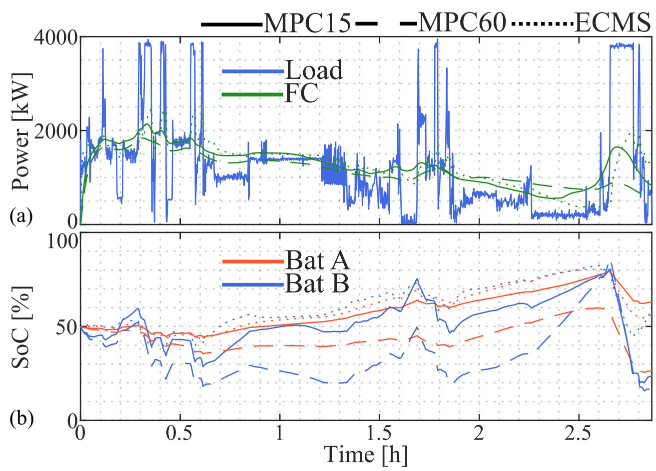


FIGURE 11. Time-series of simulation results for ECMS, and MPC with 15 min and 60 min horizon, showing (a) Total FC versus load power, (b) SoC in the ESSs.

and computational effort is within reasonable limits. Toward the end, especially around 2.5 h, the number of iterations is elevated compared to the first half of the simulation. The main reason for this lies in the high SoC of the batteries and comparably low power load. These significantly influence the steepness of the power bids as a function of the price, influencing convergence behavior of the price adjustment algorithm.

A reliable load forecast over 15 min has been proven possible in [25]. To gauge the potential benefits of an increased prediction horizon, Fig. 10 shows the costs with MPC for varying prediction horizons. The results show that the performance improves with an increasing prediction and optimization horizon. The MPC with 15 min decreases operational costs compared to the implemented instantaneous optimization by 18.3%, mainly through decreased degradation. Shortening the prediction horizon to 5 min, the costs increase by 2.7%, whereas an increase to 60 min promises a cost reduction of up to 6.0%. Hence, the differences are quite small between horizons of 5 and 15 min. However, longer horizons promise significant gains for this specific case study. This highlights the importance of long prediction horizons for improving the operational efficiency of modular SPS.

Fig. 11 compares the time-series of load power versus total FC power and battery SoC for ECMS versus MPC with 15 and 60 min horizons. Fig. 11(a) shows how volatile the power output of the FC is when using an instantaneous optimization, which immediately reacts to load changes. A predictive EMS flattens the FC power with an increasing horizon. In addition, with 60 min of prediction and optimization, the power output stays closer to the average required power than with a shorter horizon, which is more efficient with a quadratic cost function. The longer the horizon, the more extensive and effective the strategic charging of the ESS can be realized [see Fig. 11(b)].

### E. INDIVIDUAL FC STATE SWITCHING

Next, we investigate the effect of allowing an individual ON- and OFF switching of FC modules according to the method described in Section III. The parameters used for implementing the state switching heuristic are listed in Table 5.

The graphs in Fig. 12 show a comparison of the distributed MPC with 15 min prediction horizon versus the MPC

**TABLE 5. FC State Switching Heuristic Parameterization**

| Parameter | Description | Value |
|---|---|---|
| $p_{i,on}$ | On switch power threshold | $0.5P_iSoH_i$ |
| $n_{i,on}$ | On switch sample threshold | $\lceil 0.2N_h \rceil$ |
| $p_{i,off}$ | Off switch threshold | $0.2P_iSoH_i$ |

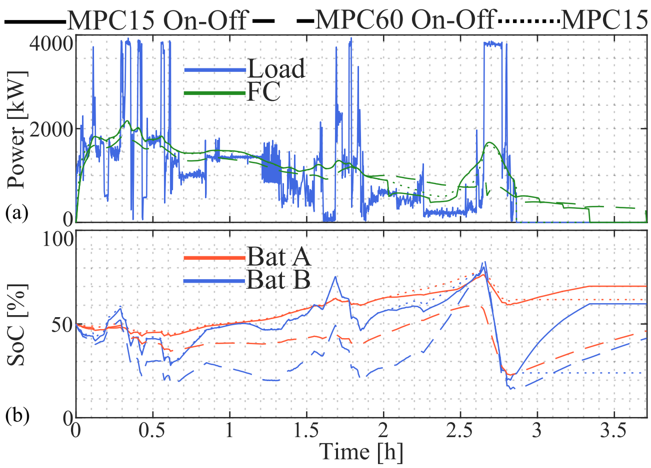


**FIGURE 12. Time-series of simulation results for MPC with 15 min horizon versus MPC with 15 and 60 min horizon and individual FC state switching, showing (a) total FC versus load power, (b) SoC in the ESSs.**

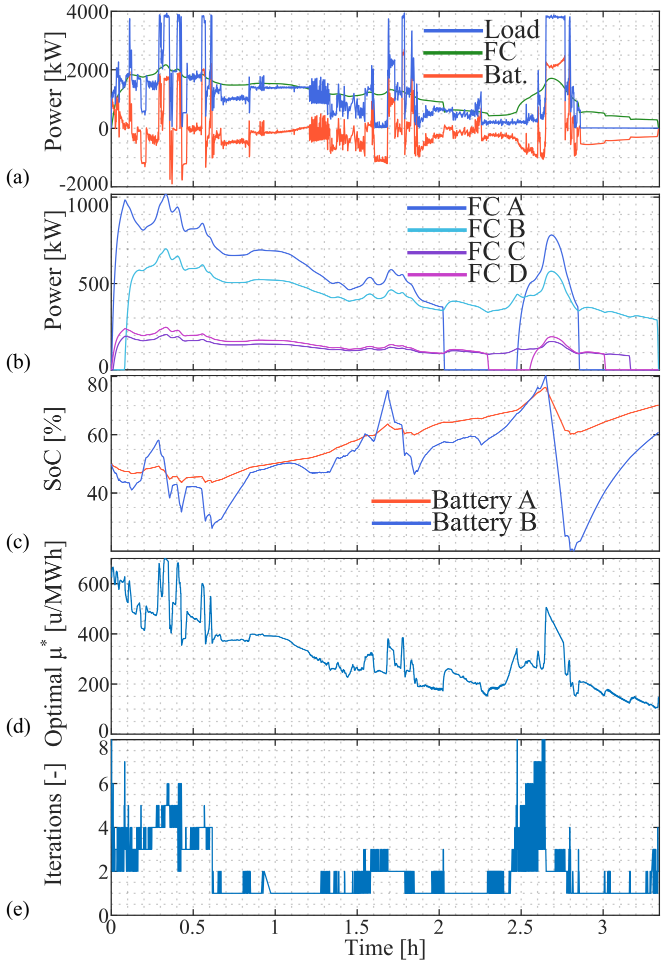


**FIGURE 13. Exemplary results for one mission profile with distributed MPC with 15 min load forecasting and individual ON–OFF switching, showing (a) the total power split, (b) FC power per module, (c) battery SoC per module, (d) the optimal price, (e) iterations required for solving the optimization.**

with added individual state-switching for horizons of 15 and 60 min. The comparison between the strategies with 15 min prediction horizon shows an overall more dynamic operation of the FC generation when enabling the state switching. The difference lies therein that the state switching is used for achieving the dynamics, whereas the strategy with all system ON is required to apply higher power gradients to achieve the dynamics. Further, the state switching allows operation at lower total loads without running individual modules at detrimental low power outputs. The new strategy with the 60 min prediction horizon shows a very flat FC generation, and an overall lower average FC loading, resulting in higher efficiency. This also results in lower SoC of the batteries due to the decreased marginal cost of power generation. At the end of the mission profile, the switching logic allows to run FC modules longer for replenishing the battery charge. It must be noted that the final SoC is subject to the switching heuristics and not a result of a deterministic target value.

Fig. 13 shows more detailed results for the same mission with the 15 min MPC including state-switching. The time-series plots show clearly when each module switches ON and OFF. The EMS allows a late start-up, an early shut-down, as well as an intermittent off-period for each module, as can be observed here. Further, the simulation is extended until all modules are switched OFF. Additional benefits from the ON–OFF switching are the avoidance of very low FC loadings, as well as an improved convergence behavior in these operation zones. The graphs lay out in detail when individual modules are switched ON and OFF, and what the effects are on power balance and on the equilibrium market price.

The results cumulated over all missions are shown in Fig. 14. This plot not only portrays the improvement of both hydrogen consumption and degradation for all horizons due to the added state-switching, but also the stark reduction in degradation costs with increasing horizon length. The MPC with 15 min horizon yields a total operation cost reduction of 3.0% by enabling the individual state switching. With 60 min, the cost reduction amounts to 12.7%. This clearly underscores the cost reduction potential that can be achieved by optimizing the ON- and OFF-switching instances of FC modules together with an extension of the prediction and optimization horizon.

### F. DEGRADATION RATES

The results of the previous sections summarize the total degradation costs from the FC modules. In addition, it is interesting to study the individual degradation rates with regard to their state-of-health. Table 6 lists each module's degradation rate

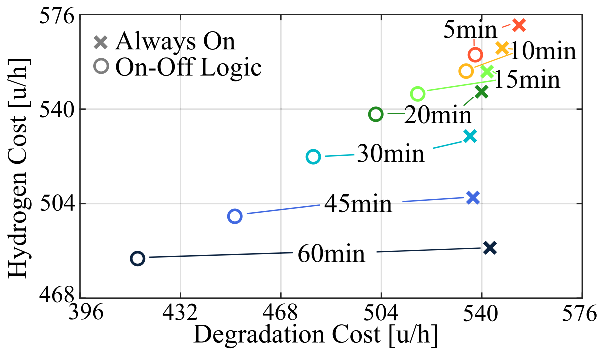


**FIGURE 14.** Accumulated hydrogen and degradation costs for distributed MPC with and without local ON–OFF switching.

**TABLE 6.** Cell Degradation Rates in $\mu$V/h for Individual FC Modules for Various EMS Settings

| | 15 min | 60 min | 15 min On-Off | 60 min On-Off |
|---|---|---|---|---|
| FC A | 10.26 | 10.25 | 10.84 | 9.45 |
| FC B | 9.87 | 9.81 | 8.62 | 5.63 |
| FC C | 9.92 | 9.88 | 9.26 | 8.79 |
| FC D | 10.12 | 10.09 | 9.87 | 9.37 |

for different prediction horizons and state switching strategy. One important observation is that there is an increasing relationship between state-of-health and degradation rate ($A > D > C > B$). This means that over time, the state of parallel FC modules balances. An additional observation is the fact that individual state switching increases the difference between the degradation rates. This can be explained by the fact that the heuristic switching keeps inefficient modules, i.e., those with lower state-of-health, switched OFF more regularly or even entirely during a mission.

## V. REAL-TIME CONTROLLER DEPLOYMENT

To demonstrate the application of the distributed energy management algorithm on multiple hardware components, we deploy the controllers on two real-time target machine (RTTM) from Speedgoat. A schematic of this setup is displayed in Fig. 15.

The functional code on one machine, the Speedgoat Performance RTTM, is split into two parts, which run in parallel but without sharing any signals. On one part, we deploy the central coordinator that runs Algorithm 1 together with function which supplies the load predictions. On the second part, the power system simulation, including primary control loops, is realized. The second machine, the Speedgoat Baseline RTTM, runs all local agents. These run in parallel, without exchanging any signals between agents.

Communication between the machines is realized via UDP/IP over Ethernet. We connect two distinct communication lines for system level interaction, i.e., agent to central coordinator, and local interfaces, i.e., agent to component. The system level communication transmits the signals between agents and central coordinator, which are required for the algorithms 2 and 1. Over the local communication line, the agents send power references, and state references for the FC to their respective local control loops. The agents receive power, SoC and fault signals back, which they require for updating their local cost functions.

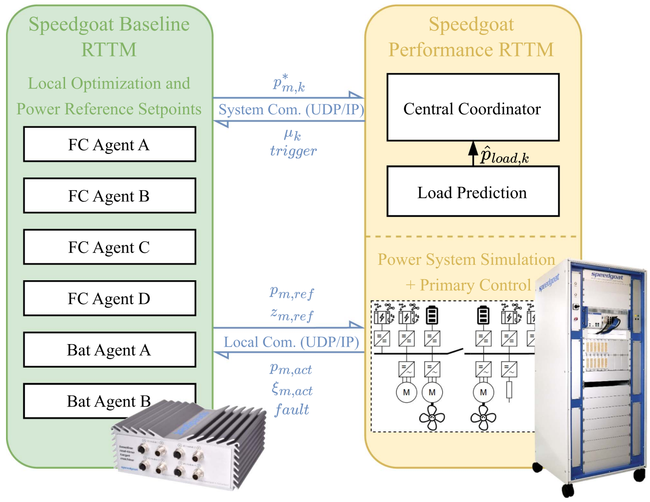


**FIGURE 15.** Deployment of distributed optimization on HiL setup with two Speedgoat real-time target machines (RTTM) and communication via UDP/IP.

**TABLE 7.** Comparison of Problem Complexity Per Instance for Centralized and Distributed Energy Management Architectures

| | **Centralized** | **Distributed** |
|---|---|---|
| Decision variables | $N_h \cdot M$ | $N_h$ |
| Equality constraints | $N_h$ | 0 |
| Inequality constraints | $4N_h \cdot M$ | $4N_h$ |
| Parallel instances | 1 | $M$ |
| Serial instances | 1 | $it$ |
| Total complexity | $\mathcal{O}((M \cdot N_h)^k)$ | $\mathcal{O}(it \cdot M \cdot N_h^k)$ |

To compare the computational complexity of the distributed and centralized architectures, Table 7 lists key attributes of the optimization problems to be solved. The considered problems have linear constraints and convex objective functions. In our implementation, both the centralized and distributed formulations reduce to quadratic programs, which minimizes computational effort. Each module has box constraints on their inputs (FC power gradient, ESS power) and states (FC power, SoC) at each interval. In the centralized formulation, the power balance constraint couples all modules at each interval. In the distributed architecture, power balance is enforced by the central coordinator and does not appear in the local problems. A centralized optimization solves a single, larger problem whose number of decision variables and constraints grows with both the module count and prediction horizon. Assuming a polynomial complexity of order $k$ in the problem size, the computational effort of the centralized approach increases nonlinearly with system size. In contrast, a distributed architecture requires many smaller problems to be solved in parallel and repeatedly. The size of these local problems is independent of the system size and it can be assumed that the number of dual gradient ascent steps $it$, is largely unaffected by the system size. The total complexity consequently scales linearly with the module count and polynomially with the horizon length. The relative advantage of one architecture over the other, and the corresponding computational requirements for the control hardware, depend on the solver implementation, scaling behavior, and additional per-instance overhead. An benefit of the distributed approach is the decoupling of local problems, which enables their parallel execution.

### A. OPTIMAL DISPATCH

For testing the distributed optimization in real time, we subject the power system to a load step. At time $t = 600\,\text{s}$, the power steps up from 1300 kW to 3800 kW, which corresponds to an operational transition from transit to high assist. For the ease of demonstrating the predictive EMS, we limit the number of MPC intervals to $N_h = 10$ and set the interval width $T_{mpc} = 30\,\text{s}$, resulting in a prediction horizon of 5 min. Further, the frequency of optimization instances is reduced with $T_{opt} = 10s$. To showcase the convergence of the iterative optimization algorithm, all $\mu_k$ are initialized with the first element $\mu_1$ at which the previous optimization instance has converged. It must be noted that this initialization method, as well as the reduced optimization frequency requires a higher number of iterations, compared to the approach described in Section III. Furthermore, we trigger a fault in FC A to capture the system response to a component fault at high, constant load. The power sharing between accumulated FC and battery power outputs against the load is displayed in Fig. 16.

The graph shows the power step occurring at 600 s. Before 300 s, the load steps enters the load prediction horizon. Before this time, only FC A has been active and slowly approached a quasi-static power sharing with the batteries. After, the FC power ramps up and the other FC modules sequentially switch ON to supply the anticipated power load. At the time of the load step, only the batteries immediately adjust their power output to the new operation point, while the FC systems continue to increase their load. At 850 s, the FC systems supply the largest share of the load when a fault in FC A is triggered. Accordingly, the total FC power drops instantly. Immediately afterward, the batteries compensate for the loss of generation and over minutes afterwards, FC and batteries find a new, efficient power dispatch. As a final note, it can be seen that the batteries' actual output power differs from the optimal reference values in-between optimization instances, and around high load steps. This is due to the batteries being utilized for instantaneous load-balancing as well as the limited optimization frequency.

### B. CONVERGENCE AT LOAD STEP

The advantage of the predictive optimization is that the algorithm can anticipate load changes before they occur. To investigate how the distributed optimization reacts to the prediction of the load step, we investigate the optimization instance occurring at time $t = 330\,\text{s}$, at which the load step is

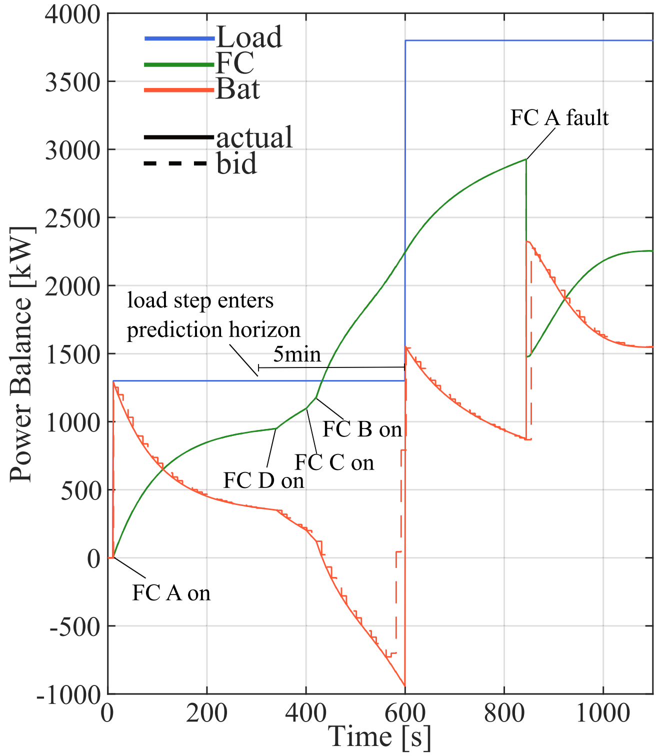


**FIGURE 16.** Cumulative FC and battery power references (final bid) and actual power for rectangular load step from 1300 to 3800 kW.

fully captured within the final MPC interval. The corresponding evolution of accumulated bids from all power system components is shown in Fig. 17. The horizontal offset of bids within each interval is only for visualization. In the time domain, the dual variables and power bids are updated with the communication period $T_{com}$, which is 100 ms here. Showcased in this campaign via UDP/IP, this bandwidth, or even significantly faster, can be realized via various communication technologies.

The plot shows that the algorithm requires 11 iterations to converge. For the first nine intervals, the initial dual variables from the previous optimization yield power bids that are sufficiently close to the power load. Only the tenth interval, for which now the stepped-up load to 3800 kW is predicted, requires multiple iterations, until the mismatch has dropped below the threshold. In accordance with the increased load requirement, the dual variable in interval 10 had to be increased significantly.

### C. CONVERGENCE AT COMPONENT FAULT

Whereas the predictive optimization is able to anticipate the load step in the previous section, a component fault is typically an unforeseen event which requires immediate action. We assume that a fault occurs in FC module A, which is the largest power supply in the system, necessitating an sudden disconnect. Accordingly, the power output of the unit is reduced to zero within a short time period, and the FC agent is

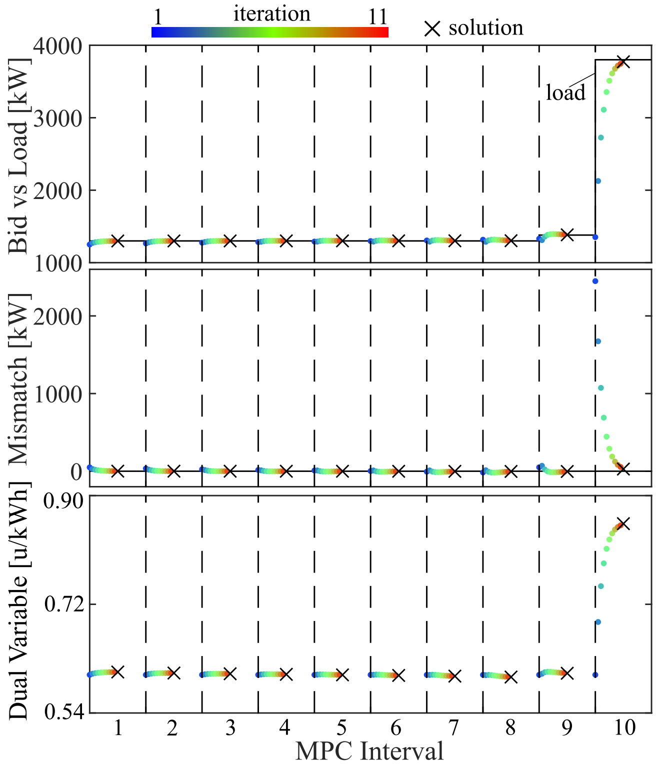


**FIGURE 17.** Convergence of distributed optimization during real-time simulation at *t*=330 s, with the load step entirely predicted in the 10th MPC interval.

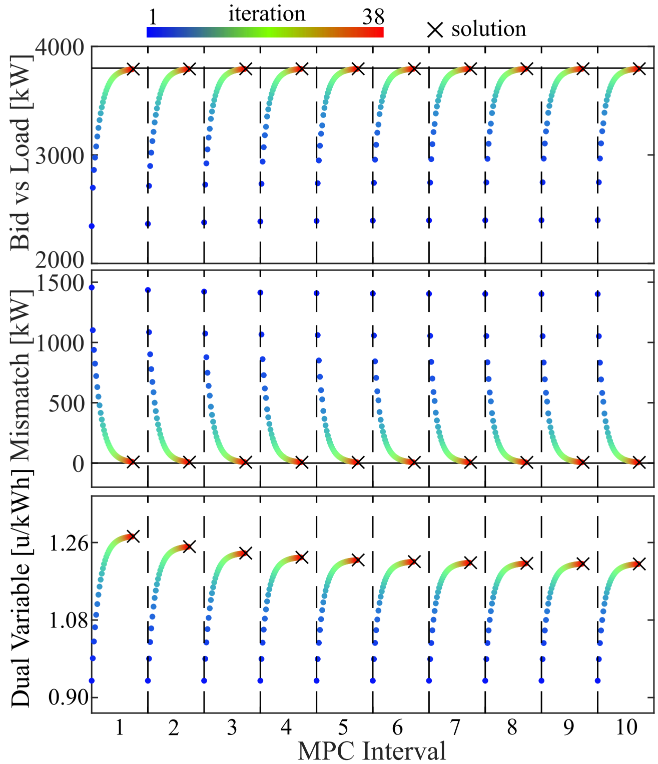


**FIGURE 18.** Convergence of distributed optimization during real-time simulation at time of FC fault (t=850 s) during full load.

bidding 0 kW. Hence, the power bids from other components must compensate for the loss of generation. Opposed to the previous case, this sudden loss leads to an imbalance in all of the optimization intervals and accordingly all initial market prices from the previous optimization instance are far away from an equilibrium. The convergence of the optimization algorithm immediately after the fault at $t = 850\,\mathrm{s}$ is shown in Fig. 18. We can observe that the algorithm requires 38 iterations until convergence. There is significant movement in all of the intervals, since the loss of one large power supply leaves a large gap between initial power bid and actual power load over the entire optimization horizon. Hence, the dual variable highly increases in all intervals. The earlier intervals yield a slightly higher marginal cost than later intervals due to the high power gradients demanded from the FC systems.

The testing of these scenarios on multiple target machines showcases that the distributed optimization via Lagrangian dual decomposition in real time, as proposed in this work, is suitable for deployment on actual control hardware. The distribution algorithm is converging in two extreme scenarios, even with nonideal starting points. An initialization with the dual variables of the previous optimization instance, as well as a less frequent occurrence of stark load changes will in practice significantly reduce the average number of iterations per optimization, as indicated by the results in Fig. 13. Finally, this demonstration underscores the adaptability of a distributed control approach for fault-tolerant system operation.

## VI. CONCLUSIONS AND DISCUSSION

Increasing focus on modularity in SPS requires power system control algorithms to become more adaptive and resilient. This article achieves this through a shift from a centralized toward a distributed control architecture. Dual decomposition and predictive control allow for a flexible and cost-optimized power dispatch, coordinated via a virtual market price. The deployment of distributed controllers and central coordinator on multiple RTTM display the applicability of a predictive, distributed energy management for SPS on actual control and communication hardware. The method's resilience is shown by demonstrating the adaptation of the optimal power dispatch at the time of a generator fault, which is met by a reoptimization of the power dispatch.

Simulation results show the long-term performance of the proposed predictive and distributed energy management approach. The distributed architecture is able to match the performance of a conventional, centralized approach. The predictive strategy is demonstrably superior to instantaneous optimization, yielding a cost reduction of 18.3% with a 15 min prediction horizon. The MPC performance increases with the horizon length, reducing operation costs by an additional 6.0% at 60 min. In addition, a local decision-making heuristic shows promising potential for the cell degradation via optimized timing of ON- and OFF switching. At 15 min, this reduces operation costs by 3.0% and at 60 min by 12.7%. The cost-optimal power dispatch respects the parameterization and constraints of each module, proving the adaptability to individual characteristics. The results indicate the added resilience, adaptability, and privacy-preserving aspect gained through the distributed architecture. Hence, distributed power system control is a promising solution for the challenges in the operation of modern ships with an all-electric and integrated power system. The adaptation to each component's characteristics and to a topology alteration underscores the modularity of this control architecture.

For future work, it is recommended to pay increased attention to the opportunities created by the distributed optimization on the component-level control. The agent-based approach allows a highly accurate representation of each component's characteristics and parameters in the local optimization. To fully leverage this, mechanisms for online parameter identification and deployment of accurate, dynamic models should be studied and integrated in the distributed framework. Further attention must be placed on the price adaptation mechanism, exploring its convergence behavior. Whereas the inclusion of convex and smooth cost functions is successfully handled with the approach presented in this study, the addition of nonconvex modules (e.g., internal combustion engines), and more complex decision-making will require more sophisticated solutions. Alternative algorithms, such as ADMM, should be explored for applications in which the Lagrangian dual decomposition and dual gradient ascent fall short. An additional consideration lies in the opportunities and challenges arising from the flexible operation of complex and modular power system designs. More specifically, a distributed control architecture is promising for handling more complex networks, e.g., with a zonal or meshed layout, that allow flexible topology reconfiguration via bus-tie switches. This warrants further studies on the design of a distributed control and energy management architecture that incorporates topology-awareness.

## REFERENCES


[1] N. Shakeri, M. Zadeh, and J. Bremnes Nielsen, "Hydrogen fuel cells for ship electric propulsion: Moving toward greener ships," *IEEE Electrific. Mag.*, vol. 8, no. 2, pp. 27–43, Jun. 2020, doi: 10.1109/MELE.2020.2985484.

[2] M. U. Mutarraf, Y. Terriche, K. A. K. Niazi, J. C. Vasquez, and J. M. Guerrero, "Energy storage systems for shipboard microgrids—A review," Energies, p. 32, Dec. 2018, doi: 10.3390/en11123492.

[3] L. Xu et al., "A Review of DC shipboard microgrids—Part I: Power architectures, energy storage, and power converters," *IEEE Trans. Power Electron.*, vol. 37, no. 5, pp. 5155–5172, May. 2022, doi: 10.1109/TPEL.2021.3128417.

[4] Y. Yuan, J. Wang, X. Yan, B. Shen, and T. Long, "A review of multi-energy hybrid power system for ships," *Renewable Sustain. Energy Rev.*, vol. 132, Oct. 2020, Art. no. 110081, doi: 10.1016/j.rser.2020.110081.

[5] L. Xu et al., "A review of DC shipboard microgrids—Part II: Control architectures, stability analysis, and protection schemes," *IEEE Trans. Power Electron.*, vol. 37, no. 4, pp. 4105–4120, Apr. 2022, doi: 10.1109/TPEL.2021.3128409.

[6] A. Latorre, T. B. Soeiro, R. Geertsma, A. Coraddu, and H. Polinder, "Shipboard DC Systems—A critical overview: Challenges in primary distribution, power-electronics-based protection, and power scalability," *IEEE Open J. Ind. Electron. Soc.*, vol. 4, pp. 259–286, Jul. 2023, doi: 10.1109/OJIES.2023.3294999.

[7] S. Qazi et al., "Powering Maritime: Challenges and prospects in ship electrification," *IEEE Electrific. Mag.*, vol. 11, no. 2, pp. 74–87, Jun. 2023, doi: 10.1109/MELE.2023.3264926.

[8] A. G. Elkafas, S. Barberis, D. T. Dong, A. Schönborn, and M. Rivarolo, "Multi-aspect assessment for the retrofitting of operating vessels in ports by using advanced power systems," *Energy Convers. Manage., X*, vol. 26, Apr. 2025, Art. no. 101011, doi: 10.1016/j.ecmx.2025.101011.

[9] A. Coraddu, S. Tamburello, C. Löffler, H. E. Ceyhun, L. van Biert, and L. Oneto, "State-of-art energy management strategies for hybrid fuel cell applications for ships," in *Proc. Fuel Cell and Hydrogen Technology in Maritime Transp.*, C. O. Colpan, S. A. Korkmaz, and O. Konur, Eds., pp. 121–178. Springer Nature Switzerland, 2025.

[10] A. Broer, H. Polinder, and L. van Biert, "Polymer electrolyte membrane fuel cell degradation in ships—Review of degradation mechanisms and research gaps," *J. Power Sources*, vol. 640, Jun. 2025, Art. no. 236678, doi: 10.1016/j.jpowsour.2025.236678.

[11] M. Jaurola, A. Hedin, S. Tikkanen, and K. Huhtala, "Optimising design and power management in energy-efficient marine vessel power systems: A literature review," *J. Mar. Eng. Technol.*, vol. 18, no. 2, pp. 92–101, May. 2019, doi: 10.1080/20464177.2018.1505584.

[12] R. Geertsma, R. Negenborn, K. Visser, and J. Hopman, "Design and control of hybrid power and propulsion systems for smart ships: A review of developments," *Appl. Energy*, vol. 194, pp. 30–54, May. 2017, doi: 10.1016/j.apenergy.2017.02.060.

[13] A. Sciarretta and L. Guzzella, "Control of hybrid electric vehicles," *IEEE Control Syst. Mag.*, vol. 27, no. 2, pp. 60–70, Apr. 2007, doi: 10.1109/MCS.2007.338280.

[14] L. C. W. Yuan, T. Tjahjowidodo, G. S. G. Lee, R. Chan, and A. K. Adnanes, "Equivalent consumption minimization strategy for hybrid all-electric tugboats to optimize fuel savings," in *Proc. Amer. Control Conf.*, Boston, MA, USA, vol. 2016, Jul. 2016, pp. 6803–6808, doi 10.1109/ACC.2016.7526743.

[15] L. C. W. Yuan, T. Tjahjowidodo, G. G. L. Seet, and R. Chan, "Implementation of optimization-based power management for all-electric hybrid vessels," *IEEE Access*, vol. 6, pp. 74339–74354, Nov. 2018, DOI: 10.1109/ACCESS.2018.2883324.

[16] Z. Zhang, C. Guan, and Z. Liu, "Real-time optimization energy management strategy for fuel cell hybrid ships considering power sources degradation," *IEEE Access*, vol. 8, pp. 87046–87059, Apr. 2020, doi: 10.1109/ACCESS.2020.2991519.

[17] T. Kopka, C. Löffler, A. Coraddu, and H. Polinder, "Hierarchical control strategy for fuel cell-battery shipboard power system utilizing a modular control architecture," in *Proc. IEEE Transp. Electrific. Conf. Expo, Asia-Pacific*, Chiang-Mai, Thailand, Nov. 2023, doi: 10.1109/ITECAsia-Pacific59272.2023.10372342.

[18] J. Hu, Y. Shan, J. M. Guerrero, A. Ioinovici, K. W. Chan, and J. Rodriguez, "Model predictive control of microgrids–An overview," *Renewable Sustain. Energy Rev.*, vol. 136, Feb. 2021, Art. no. 110422, doi: 10.1016/j.rser.2020.110422.

[19] P. Xie, S. Tan, J. M. Guerrero, and J. C. Vasquez, "MPC-informed ECMS based real-time power management strategy for hybrid electric ship," *Energy Rep.*, vol. 7, pp. 126–133, Apr. 2021, doi: 10.1016/j.egyr.2021.02.013.

[20] T. L. Vu, A. A. Ayu, J. S. Dhupia, L. Kennedy, and A. K. Adnanes, "Power management for electric tugboats through operating load estimation," *IEEE Trans. Control Syst. Technol.*, vol. 23,, no. 6, pp. 2375–2382, Nov. 2015, doi: 10.1109/TCST.2015.2399440.

[21] G. Seenumani, J. Sun, and H. Peng, "A hierarchical optimal control strategy for power management of hybrid power systems in all electric ships applications," in *Proc. 49th IEEE Conf. Decis. Control*, Atlanta, GA, USA, pp. 3972–3977, Dec. 2010, doi: 10.1109/CDC.2010.5717035.

[22] A. Haseltalab, F. Wani, and R. R. Negenborn, "Multi-level model predictive control for all-electric ships with hybrid power generation," *Int. J. Elect. Power Energy Syst.*, vol. 135, Feb. 2022, Art. no. 107484, doi: 10.1016/j.ijepes.2021.107484.

[23] L. Yuan, T. Tjahjowidodo, G. S. G. Lee, and R. Chan, "Optimizing fuel savings and power system reliability for all-electric hybrid vessels using model predictive control," in *Proc. IEEE Int. Conf. Adv. Intell. Mechatron.*, Munich, Germany, pp. 1532–1537, Jul. 2017, doi: 10.1109/AIM.2017.8014236.

[24] Y. Zhang, Q. Xue, D. Gao, W. Shi, and W. Yu, "Two-level model predictive control energy management strategy for hybrid power ships with hybrid energy storage system," *J. Energy Storage*, vol. 52, Aug. 2022, Art. no. 104763, doi: 10.1016/j.est.2022.104763.

[25] T. Kopka, S. Tamburello, L. Oneto, L. van Biert, H. Polinder, and A. Coraddu, "Degradation-aware predictive energy management for fuel cell-battery ship power system with data-driven load forecasting," Apr. 2026, doi: 10.48550/arXiv.2604.14994.

[26] D.-L. Nguyen and H.-H. Lee, "A survey on cooperative control strategies for DC microgrids," *Neurocomputing*, vol. 486,, pp. 225–236, May. 2022, doi: 10.1016/j.neucom.2021.11.036.

[27] P. Xie et al., "A distributed real-time power management scheme for shipboard Zonal multi-microgrid system," *Appl. Energy*, vol. 317, Jul. 2022, Art. no. 119072, DOI 10.1016/j.apenergy.2022.119072.

[28] N. Doerry and K. McCoy, "Next generation integrated power system: NGIPS technology development roadmap," *Defense Tech. Inf. Center*, Fort Belvoir, VA, Tech. Rep., Nov. 2007.

[29] A. Feliachi, K. Schoder, S. Ganesh, and H.-J. Lai, "Distributed control agents approach to energy management in electric shipboard power system," in *Proc. IEEE Power Eng. Soc. Gen. Meeting*, Montreal, QC, Canada, Jun. 2006, doi: 10.1109/PES.2006.1708943.

[30] G. Sulligoi, A. Vicenzutti, and R. Menis, "All-electric ship design: From electrical propulsion to integrated electrical and electronic power systems," *IEEE Trans. Transp. Electrific.*, vol. 2, no. 4, pp. 507–521, Dec. 2016, DOI 10.1109/TTE.2016.2598078.

[31] K. Lai and M. S. Illindala, "A distributed energy management strategy for resilient shipboard power system," *Appl. Energy*, vol. 228, pp. 821–832, Oct. 2018, doi: 10.1016/j.apenergy.2018.06.111.

[32] S. Vedula, S. S. Alaviani, and O. M. Anubi, "Distributed model-predictive energy management strategy for shipboard power systems considering battery degradation," *IFAC-PapersOnLine*, vol. 58, no. 28, pp. 360–365, Jan. 2024, doi: 10.1016/j.ifacol.2025.01.061.

[33] T. Kopka, A. Coraddu, and H. Polinder, "Optimal energy management of FC-battery shipboard power system using dynamic programming," in *Proc. IEEE Int. Conf. Elect. Syst. Aircraft, Railway, Ship Propulsion Road Veh. Int. Transp. Electrific. Conf.*, Naples, Italy, Nov. 2024, doi: 10.1109/ESARS-ITEC60450.2024.10819881.

[34] Y. Wang, S. Mondal, K. Satpathi, Y. Xu, S. Dasgupta, and A. K. Gupta, "Multiagent distributed power management of dc shipboard power systems for optimal fuel efficiency," *IEEE Trans. Transp. Electrific.*, vol. 7, no. 4, pp. 3050–3061, Dec. 2021, doi: 10.1109/TTE.2021.3086303.

[35] K. K. Tafanidis, K. D. Taxeidis, F. D. Kanellos, and G. J. Tsekouras, "Optimal operation of war-ship electric power system equipped with energy storage system," *J. Comput. Model.*, vol. 3, no. 4, pp. 41–60, 2013.

[36] J. Hu, M. Z. Q. Chen, J. Cao, and J. M. Guerrero, "Coordinated active power dispatch for a microgrid via distributed Lambda iteration," *IEEE Trans. Emerg. Sel. Topics Circuits Syst.*, vol. 7, no. 2, pp. 250–261, Jun. 2017, doi: 10.1109/JETCAS.2017.2676019.

[37] S. Luo, K. Peng, C. Hu, and R. Ma, "Consensus-based distributed optimal dispatch of integrated energy microgrid," *Electron.*, vol. 12, no. 6, Jan. 2023, Art. no. 1468, doi: 10.3390/electronics12061468.

[38] T. C. J. Romijn, T. H. Pham, and S. Wilkins, "Modular ECMS framework for hybrid vehicles," *IFAC-PapersOnLine*, vol. 52, no. 5, pp. 128–133, Jan. 2019, doi: 10.1016/j.ifacol.2019.09.021.

[39] K. Huang, S.K. Srivastava, D. A. Cartes, and L.-H. Sun, "Market-based multiagent system for reconfiguration of shipboard power systems," *Elect. Power Syst. Res.*, vol. 79, no. 4, pp. 550–556, Apr. 2009, doi: 10.1016/j.epsr.2008.06.020.

[40] X. Feng, K. L. Butler-Purry, and T. Zourntos, "Multi-agent system-based real-time load management for all-electric ship power systems in DC zone level," *IEEE Trans. Power Syst.*, vol. 27, no. 4, pp. 1719–1728, Nov. 2012, doi: 10.1109/TPWRS.2012.2194314.

[41] Y. Zhang, Q. Shan, F. Teng, and T. Li, "Coordinated energy management scheme for ship-harbour energy system based on economic optimal scheduling," in *Proc. Int. Conf. Security, Pattern Analysis, Cybern.*, Chengdu, China, pp. 81–86, Jun. 2021, doi: 10.1109/SPAC53836.2021.9539984.

[42] G. Chen and Q. Yang, "An ADMM-based distributed algorithm for economic dispatch in islanded microgrids," *IEEE Trans. Ind. Inform.*, vol. 14, no. 9, pp. 3892–3903, Sep. 2018, doi: 10.1109/TII.2017.2785366.

[43] T. V. Vu et al., "Large-scale distributed control for MVDC ship power systems," in *Proc. 44th Annu. Conf. IEEE Ind. Electron. Soc.*, Washington, DC, USA, pp. 3431–3436, Oct. 2018, doi: 10.1109/IECON.2018.8591346.

[44] C. S. Edrington et al., "Distributed energy management for ship power systems with distributed energy storage," *J. Mar. Eng. Technol.*, vol. 19, no. sup1, pp. 31–44, Jan. 2020, doi: 10.1080/20464177.2019.1684122.

[45] Y. Zhang, Q. Shan, F. Teng, and T. Li, "Distributed economic optimal scheduling scheme for ship-integrated energy system based on load prediction algorithm," *Front. Energy Res.*, vol. 9, Sep. 2021, doi: 10.3389/fenrg.2021.720374.

[46] T. Fletcher, R. Thring, and M. Watkinson, "An energy management strategy to concurrently optimise fuel consumption & PEM fuel cell lifetime in a hybrid vehicle," *Int. J. Hydrogen Energy*, vol. 41, no. 46, pp. 21503–21515, Dec. 2016, doi: 10.1016/j.ijhydene.2016.08.157.

[47] H. Chen, P. Pei, and M. Song, "Lifetime prediction and the economic lifetime of proton exchange membrane fuel cells," *Appl. Energy*, vol. 142, pp. 154–163, Mar. 2015, doi: 10.1016/j.apenergy.2014.12.062.

[48] F. A. de Bruijn, V. a. T. Dam, and G. J. M. Janssen, "Review: Durability and degradation issues of PEM fuel cell components," *Fuel Cells*, vol. 8, no. 1, pp. 3–22, Feb. 2008, doi: 10.1002/fuce.200700053.

[49] K. Meng, H. Zhou, B. Chen, and Z. Tu, "Dynamic current cycles effect on the degradation characteristic of a H2/O2 proton exchange membrane fuel cell," *Energy*, vol. 224, Jun. 2021, Art. no. 120168, doi: 10.1016/j.energy.2021.120168.

[50] S. Tamburello et al., "Preliminary methodology assessment for PEMFC durability testing in transport applications," *Electrochimica Acta*, vol. 554, Apr. 2026, Art. no. 148267, doi: 10.1016/j.electacta.2026.148267.

[51] Nedstack, "Nedstack FCS 13-XXL," Jul. 2023. [Online]. Available: https://nedstack.com/sites/default/files/2019-11/20191105_nedstack_fcs_13-xxl.pdf

[52] G. Kleen and W. Gibbons, "DOE hydrogen program record: Heavy-duty fuel cell system cost–2023," Aug. 2024. [Online]. Available: https://www.hydrogen.energy.gov/docs/hydrogenprogramlibraries/pdfs/ review24/24004-hd-fuel-cell-system-cost-2023.pdf

[53] J. M. Walker, A. Coraddu, and L. Oneto, "Power demand forecasting for a hybrid marine energy system with shallow and deep learning," in *Proc. OCEANS*, pp. 1–8, Apr. 2024, doi: 10.1109/OCEANS51537.2024.10682263.

[54] T. Kopka, A. Coraddu, and H. Polinder, "Distributed MPC for cost-optimal control of FC-battery shipboard microgrids," in *Proc. IEEE Seventh Int. Conf. DC microgrids*, Tallinn, Estonia, pp. 1–6, Jun. 2025, doi: 10.1109/ICDCM63994.2025.11144727.

[55] T. Kopka, A. Latorre, A. Coraddu, and H. Polinder, "Energy-based voltage stabilization in DC shipboard power systems with dual loop control," *IEEE Access*, vol. 13, pp. 117105–117118, Jul. 2025, doi: 10.1109/ACCESS.2025.3586382.

**TIMON KOPKA** received the B.Sc. and M.Sc. degrees in electric energy technology from RWTH Aachen University, Aachen, Germany, in 2015 and 2018, respectively. He received the M.Sc degree in electric power engineering from KTH Royal Institute of Technology, Sweden, in 2018, within the T.I.M.E. double degree program. He is currently working toward the Ph.D. degree in power system control and energy management for electrified ship power systems with Delft University of Technology, Delft, The Netherland.

From 2019 to 2022, he was a Development Engineer for Control and Drive Systems in automotive applications at LSP GmbH in Munich, Germany. In 2022, he joined the Department of Maritime and Transport Technology, Delft University of Technology. His research interests include power system control, DC microgrids, shipboard power systems, renewable energy generation, energy storage systems, and fuel cell technology. He focuses on distributed and cooperative control and optimization methods for electric power system operation.

**ANDREA CORADDU** (Senior Member, IEEE) was born in Pietrasanta, in 1979. He received the Laurea degree in naval architecture and marine engineering from the University of Genoa, Italy, in 2006, and the Ph.D. degree from the School of Fluid and Solid Mechanics, University of Genoa, in 2012, with the thesis “Modelling and Control of Naval Electric Propulsion Plants”.

He is currently an Associate Professor of intelligent and sustainable energy systems with the Maritime and Transport Technology Department, Delft University of Technology, Delft, The Netherlands. From 2020 to 2021, he was an Associate Professor with the Department of Naval Architecture, Ocean & Marine Engineering, University of Strathclyde. His relevant professional and academic experiences include working as an Assistant Professor with the University of Strathclyde, Research Associate with the School of Marine Science and Technology, Newcastle University, Research Engineer as part of the DAMEN R&D Department based in Singapore and as a Postdoctoral Research Fellow with the University of Genoa. He is also involved in several successful Grant applications from Research Councils, Industry, and International Governmental agencies focusing on the design, integration, and control of complex Marine Energy and Power Management Systems enabling the development of next-generation complex and multifunction vessels that can meet the pertinent social challenges regarding the environmental impact of human-related activities.

**HENK POLINDER** (Senior Member, IEEE) received the Ph.D. degree in electrical engineering from the Delft University of Technology, Delft, The Netherlands, in 1998.

Since 1996, he has been an Assistant/Associate Professor with the Delft University of Technology, working in the field of electrical machines and drives. From 1998 to 1999, he worked part-time in industries, with the wind turbine manufacturer Lagerwey, Barneveld, The Netherlands. In 2001, he was with Philips CFT, Eindhoven, The Netherlands. In 2008, he was with ABB Corporate Research, Västerås, Sweden. He was a Visiting Scholar with Newcastle University, Newcastle, upon Tyne, U.K., in 2002; Laval University, Quebec, QC, Canada, in 2004; the University of Edinburgh, Edinburgh, U.K., in 2006; and the University of Itajubá, Itajubá, Brazil, in 2014. He has authored or coauthored more than 250 publications. His main research interests include electric drive and energy systems for maritime applications and offshore renewables.